Direct electrical detection of DNA synthesis

Nader Pourmand*†‡, Miloslav Karhanek*†, Henrik H. J. Persson*, Chris D. Webb§, Thomas H. Lee¶, Alexandra Zahradníková‖, and Ronald W. Davis*‡

*Stanford Genome Technology Center, Stanford University, Palo Alto, CA 94304; §School of Medicine and ¶Center for Integrated Systems, Stanford University, Stanford, CA 94305; and ‖Institute of Molecular Physiology and Genetics, Slovak Academy of Sciences, Bratislava 845 07, Slovakia

Contributed by Ronald W. Davis, February 28, 2006

Rapid, sequence-specific DNA detection is essential for applications in medical diagnostics and genetic screening. Electrical biosensors that use immobilized nucleic acids are especially promising in these applications because of their potential for miniaturization and automation. Current DNA detection methods based on sequencing by synthesis rely on optical readouts; however, a direct electrical detection method for this technique is not available. We report here an approach for direct electrical detection of enzymatically catalyzed DNA synthesis by induced surface charge perturbation. We discovered that incorporation of a complementary deoxynucleotide (dNTP) into a self-primed single-stranded DNA attached to the surface of a gold electrode evokes an electrode surface charge perturbation. This event can be detected as a transient current by a voltage-clamp amplifier. Based on current understanding of polarizable interfaces, we propose that the electrode detects proton removal from the 3′-hydroxyl group of the DNA molecule during phosphodiester bond formation.

biosensors | charge perturbation detection | polymerization

The label-free, electronic detection of DNA synthesis, without the use of specialized reagents, would greatly simplify the sequencing-by-synthesis technique and accelerate its implementation for rapid DNA sequencing and diagnostics. In this article, we describe the label-free electrical detection method, charge perturbation detection (CPD), applied to sequencing by synthesis, and we discuss its underlying principles. Application of this method could be used to detect any enzymatic DNA or RNA synthesis as well as other biochemical reactions based on similar principles.

Self-priming, single-stranded DNA molecules were immobilized on the surface of a gold electrode through a thiol-reactive self-assembled monolayer. The electrode was equilibrated with 10 units of the Klenow (exo$^-$) fragment (KF) of DNA polymerase. Fig. 1*A* shows the signal resulting from the addition of a solution containing a single dNTP (1 mM concentration in the final solution volume) complementary to the nucleotide in the template sequence (top black trace). With no measurable delay, the current rises to a peak of ≈400 pA within ≈50 ms, decreases rapidly to ≈50 pA, and then shows a further, slower transient increase to ≈150 pA within 300 ms. The current transient is almost completed at 1 s (<5% of the peak current). The integral of the measured current is 87 pC (pA·s), corresponding to nucleotide incorporation to $\approx 6.0 \times 10^{11}$ DNA molecules per cm^2 of the electrode. In contrast, if a solution containing a noncomplementary dNTP was added, no current transient was observed (Fig. 1*A*, blue trace). No signal was produced when the complementary dNTP was added in the absence of DNA polymerase (green trace), in the absence of DNA (magenta trace), or if DNA was not immobilized on the electrode surface (orange trace). The lack of a detectable signal in the control experiments demonstrates the clear dependence of the current transient on the complementarity of the actual nucleotide and on the simultaneous presence of KF and immobilized DNA. The current waveform observed can therefore be attributed to the signal resulting from the incorporation of the nucleotide into the primer strand.

The DNA polymerase-catalyzed elongation of the synthesized strand proceeds by the S_N2 (bimolecular nucleophilic substitution) mechanism, which has been studied extensively (1–3). When each nucleotide is incorporated, the total negative electrical charge on the DNA molecule undergoes a net increase of $1e^-$, produced by the removal of a proton from the 3′-OH group of the DNA primer during the catalytic step of the reaction (4). The overall process is shown schematically in Fig. 2.

Because of the principle of charge conservation, the increase of the total negative charge on the DNA molecules is compensated exactly by an increase of the total positive charge in the solution caused by an increase of the proton concentration. Each of these electrical charges induces a surface charge, opposite in sign (5, 6), on the coated, electrically isolated but highly polarizable gold electrode. The magnitude of any induced charge is a function of the electrode surface geometry and the distance between the electrode and the inducing charge. For electrodes used in these experiments, the magnitude of the induced charge is effectively constant for separation distances in the range of ≈1 nm up to ≈30 μm (the detection zone), and it decreases steeply for distances >30 μm (Fig. 1*B*) (5, 6). The charges on the DNA molecule attached to the electrode are fixed locally in close proximity to the electrode surface (<100 nm), whereas the protons released from DNA are free to diffuse in the solution. For the duration of the experiment (≈1 s), the diffusion distance of protons is >136 μm (the diffusion coefficient of proton D_{H^+} in water is 9.3×10^{-5} cm^2·s^{-1}) (7). Lateral proton diffusion might be significantly faster because of specific surface hydration of the electrode and the surrounding silane layer (8, 9). The protons are thus able to diffuse far enough to produce a change of the net charge in the detection zone resulting from the immobilized negative charge on the DNA backbone. This event induces a charge sensed by the polarizable electrode. Because the electrode is held at a constant potential, the charge induced by an individual molecule results in a small pulse of current in the electrode. The sum of these current pulses from all DNA molecules attached to the electrode surface produces a large transient current detected by the voltage-clamp amplifier. Ideally, the measured current is equal to the time rate of change in net charge within the detection zone during the reaction, expressed by the equation $I(t) = dQ(t)/dt$, where Q is charge, I is current, and t is time. To evaluate the actual efficiency of signal transduction, we measured surface DNA density by polymerization of radiolabeled dCTP. This result showed that ≈1 fmol of DNA was immobilized on the electrode surface (0.0009 cm^2), which corresponds to $\approx 6.7 \times 10^{11}$ DNA molecules per cm^2 of the electrode. This result also correlates well with the calculated DNA surface density, $\approx 6.0 \times 10^{11}$ molecules per cm^2, based on the size of the electronic CPD signal of polymerization, indicat-

Conflict of interest statement: No conflicts declared.

Abbreviations: CPD, charge perturbation detection; e, electron; KF, Klenow (exo$^-$) fragment.

†N.P. and M.K. contributed equally to this work.

‡To whom correspondence may be addressed. E-mail: pourmand@stanford.edu or dbowe@stanford.edu.

www.pnas.org/cgi/doi/10.1073/pnas.0601184103

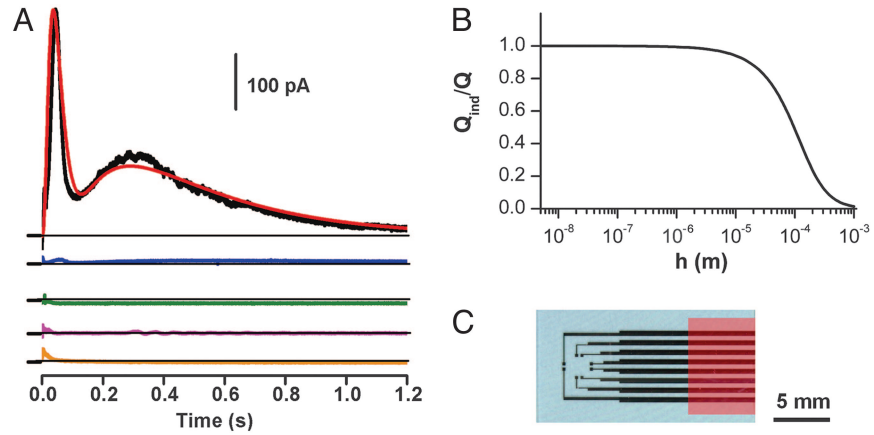

Fig. 1. Experiment and CPD chip fabrication. (*A*) Electrode current transient in response to dNTP addition. Black trace, addition of a dNTP complementary to the nucleotide in the template sequence; blue trace, addition of a noncomplementary dNTP; green trace, addition of a complementary dNTP in the absence of DNA polymerase; magenta trace, addition of a dNTP in the absence of DNA; orange trace, addition of a complementary dNTP when DNA is not immobilized, and polymerase is present; red trace, kinetic simulation (see Fig. 3). Horizontal lines next to the traces indicate the levels of zero current. (*B*) Relative induced charge (Q_{ind}/Q) for the electrode surface geometry ($x = 0.3$ mm, $y = 0.3$ mm) as a function of the distance h between the electrode and the charge Q in the solution. In the range of ≈1 nm to ≈30 μm, the electrode response does not depend on the distance between the electrode and the ion. Therefore, the changes in the immobilized charge can produce a change of the induced charge on the electrode only if the released countercharge diffuses to a distance of >30 μm. (*C*) CPD chip. An electrode chip is shown with four pairs of electrodes, connection pathways, and pads on a quartz wafer.

ing that the efficiency of signal transduction of the CPD electrode is very high.

The observed signal-to-noise ratio in the CPD signal was ≈200 (peak/rms). To obtain a 95% confidence interval, with four standard deviations, the calculated signal-to-noise ratio is effectively 50. Therefore, a rough estimate of the minimum detectable number of DNA molecules is ≈1.2×10^{10} DNA molecules per cm^2. With a standard electrode size of 0.0009

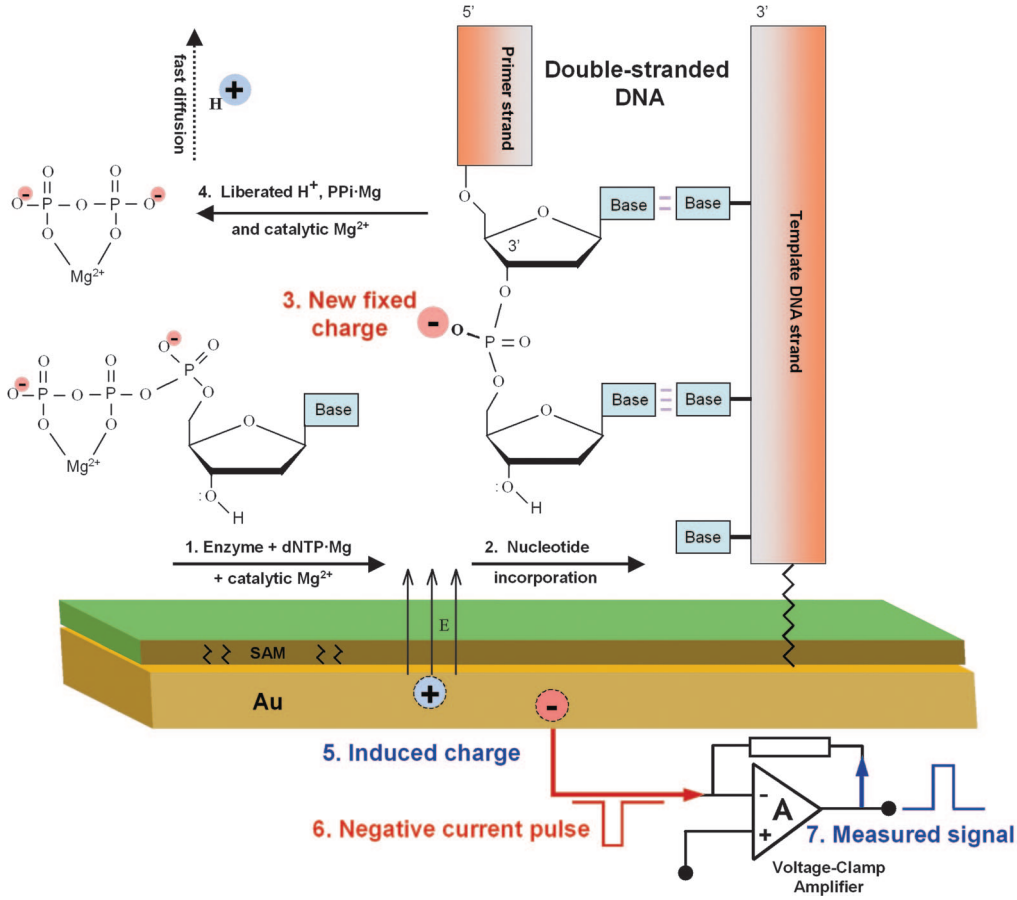

Fig. 2. Detection mechanism. The incoming dNTP molecule, complexed with one Mg^{2+} ion (28), increases the negative charge by $2e^-$. Incorporation of the catalytic Mg^{2+} ion (29) decreases the negative charge by $2e^-$ (step 1). Incorporation of nucleotide (step 2) then increases a negative charge by $1e^-$ on the new backbone phosphate group (step 3), produced by removal of a proton from the 3′-OH group of the DNA primer during the catalytic step of the reaction (step 4), followed by rapid diffusion of the proton into the surrounding solution (step 4). The change in the induced charge (step 5) can be detected by the electrode as a transient current (step 6) measured by a voltage-clamp amplifier (step 7). The diffusion distance of low-molecular-weight compounds (Mg^{2+}, Mg·dNTP^{2-}, MgPP$_i^{2-}$) in solution during the time course of the experiment (1 s) is approximately an order of magnitude slower than proton diffusion (30). For this reason the charge changes induced by most of the reaction steps (binding of the dNTP molecule, complexed with one Mg^{2+} ion, incorporation of the catalytic Mg^{2+} ion, dissociation of the catalytic Mg^{2+} ion, and of the leaving Mg^{2+}-bound pyrophosphate) do not produce a measurable electrode response. On the same basis, the Brownian motion of ions in the solution as well as conformational changes of the immobilized enzyme and DNA molecules do not produce changes in the induced charge.

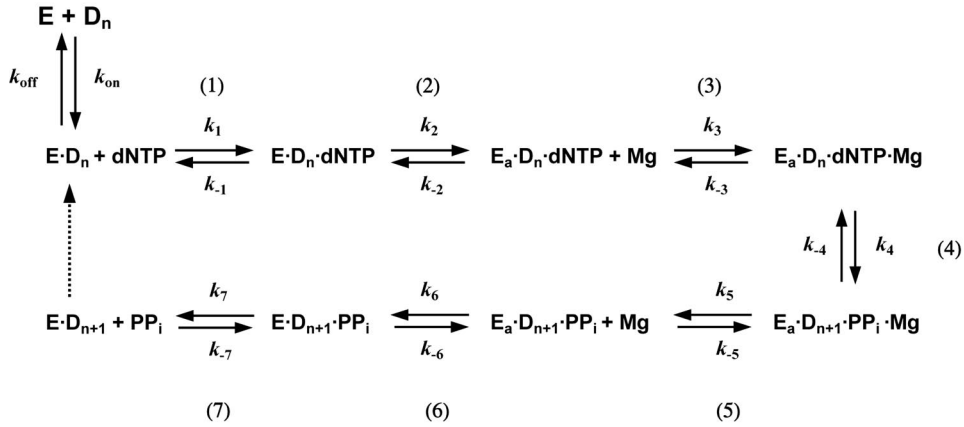

Fig. 3. Kinetic scheme. The kinetic mechanism of nucleotide incorporation by DNA polymerase is shown. The enzyme initially forms a binary complex with the DNA primer–template ($E{\cdot}D_n$). When dNTP is added to the solution, the initial binding of an incoming complementary dNTP to polymerase produces a ternary substrate complex (step 1). After this step, the enzyme undergoes a subdomain motion to form a so-called closed or active state (step 2), which is followed by binding of the catalytic Mg^{2+} ion (step 3) and by the chemical reaction of dNTP incorporation onto the DNA primer strand by the formation of a phosphodiester bond (step 4). Unbinding of the catalytic Mg^{2+} ion (step 5) is followed by a second subdomain motion of the polymerase–product complex, resulting in an open state (step 6) followed by the release of pyrophosphate PP_i (step 7) and subsequent DNA translocation. E, enzyme; E_a, active enzyme; D_n, DNA with enzyme at the nth nucleotide; k_n, kinetic rate. (Kinetic rates for red trace in Fig. 1*A*: $k_{on} = 1.2 \times 10^7\ M^{-1}{\cdot}s^{-1}$, $k_{off} = 0.06\ s^{-1}$, $k_1 = 1.25 \times 10^7\ M^{-1}{\cdot}s^{-1}$, $k_{-1} = 250\ s^{-1}$, $k_2 = 50\ s^{-1}$, $k_{-2} = 3\ s^{-1}$, $k_3 = 9.5 \times 10^5\ M^{-1}{\cdot}s^{-1}$, $k_{-3} = 100\ s^{-1}$, $k_4 = 150\ s^{-1}$, $k_{-4} = 40\ s^{-1}$, $k_5 = 100\ s^{-1}$, $k_{-5} = 9.5 \times 10^5\ M^{-1}{\cdot}s^{-1}$, $k_6 = 4\ s^{-1}$, $k_{-6} = 4\ s^{-1}$, $k_7 = 60\ s^{-1}$, $k_{-7} = 1.45 \times 10^4\ M^{-1}{\cdot}s^{-1}$.)

cm^2, this number equates to $\approx 1.8 \times 10^7$ DNA molecules (0.02 fmol of DNA).

Approximately 30% of fabricated and treated electrodes were functional, with all interface components assembled properly for detection of a DNA polymerization signal with the signal-to-noise ratio mentioned above. That 70% failed to produce any signal at all could be the result of a number of factors, including small variations in the fabrication process that result in radical changes of the CPD electrode interface. The functional electrodes are easily detected by a standardized capacitance measurement before use in an experiment (data not shown). Those that fail the capacitance test are not used for any experiments.

To gain further insight into the mechanisms underlying CPD during a single step of the KF-catalyzed reaction, we examined its kinetics (3, 10–15). The kinetic scheme based on these studies is shown in Fig. 3. Based on this kinetic model, a simulation was performed to confirm whether this underlying mechanism accounts for the signal dynamics observed. The initial enzyme–DNA binding step was assumed to be in equilibrium during the simulation because the enzyme was incubated for more than 2 min with the DNA attached to the electrode in the experiments. The published rate constants of individual reaction steps were used as the starting point of simulations, with the exception of steps 3 and 5, for which we found no published KF rate constants. We approximated these steps with $K_d \approx 100\ \mu M$ based on the published rate constants for DNA polymerase β (13). We achieved a best fit between model and experimental signals by adjustment of selected kinetic rates (in particular, k_6, k_{-6}, k_7, and k_{-7} were changed somewhat from the values published in refs. 1 and 14 to account for different experimental conditions). The red trace in Fig. 1*A* shows the time course of $d(E{\cdot}D_{n+1}{\cdot}PP_i)/dt$, an intermediate product of step 6 normalized to the maximum of the experimental signal. By using the model of Arndt *et al.* (15), an approximation for the rate of binding of Mg^{2+} and with the adjusted rate constants, we have re-created the key features of the signal dynamics, mainly the timing of the peaks of polymerization, which closely match in both the simulation and the experiment.

In summary, we demonstrated that direct label-free detection of electric charge perturbations during a DNA polymerase-catalyzed reaction is possible by using a coated gold electrode with immobilized DNA and a voltage-clamp amplifier. The CPD concept is based on the charge conservation principle and the induced surface charge of the polarizable electrode. As a result, the immobilized negative charge accumulated on the DNA backbone can be detected as soon as the positive proton leaves the detection zone, which occurs in a relatively short period of time. In principle, DNA synthesis confined to the detection zone could be detected without DNA immobilization because the protons diffuse faster than the DNA molecules.

Several techniques are available now for sequence determination. Methods involving detection and sequencing by synthesis techniques require several enzymatic and/or photochemical steps (16–18). Sequence detection by hybridization can use electrochemical reactions to detect direct electronic signals generated by DNA hybridization at the electrode surface (19–21). The label-free electrical detection method demonstrated here takes the best aspects of each of these techniques, by using the label-free approach of electrochemical detection and the more specific approach of sequencing by synthesis.

CPD experiments were performed simultaneously with two voltage-clamp electrodes, with undetectable crosstalk between electrodes 300 μm apart. The nature of the CPD reaction involves simultaneous measurement; thus, expansion requires multiple amplifiers working in parallel. Sixteen-channel voltage-clamp amplifiers are commercially available in various configurations (e.g., PatchXpress 7000A; Axon Instruments, Union City, CA) (22), readily enabling the CPD system to have multiple electrodes.

Charge perturbation detection lends itself to many additional applications because of its advantages, mainly label-free and electronic-based detection. It can be easily expanded to a multiple-electrode system, resulting in a high-throughput, compact device. Additional applications of CPD include rapid and sensitive detection of biological pathogens or genetic mutations and identification of unknown DNA sequences. CPD can also be used for general measurement of enzymes undergoing similar catalytic reactions. The CPD electrode thus potentially represents a very robust and effective biosensor for many molecular and diagnostic applications.

Materials and Methods

Fabrication of Gold Chips. The electrically active 1- × 2-cm gold chips (shown in Fig. 1*C*) were manufactured by using a semiconductor-

processing technique on a ≈10-cm-diameter wafer at the Stanford Nanofabrication Facility (SNF) (http://snf.stanford.edu). The process requires only a single mask, designed on an industry-standard computer-aided design program and produced on a piece of Mylar thin film. A 500-μm-thick quartz layer was used as the substrate. The process flow is as follows. A very thin layer of chromium was first deposited to improve the adhesion between the gold and the quartz. Next, a 1,000-Å-thick gold layer was deposited to define the pattern for both the electrodes and the connecting pads. The minimum feature size of this chip was 200 μm. To prevent contamination after processing, a 7-μm-thick photoresistor was used as a protection layer. After dicing, the photoresist was washed off with acetone and isopropyl alcohol. The chips consisted of four pairs of rectangular gold electrodes that were 0.09 mm^2 with 0.5-mm center-to-center spacing. Other areas on the chip were used for the connection pads to external devices.

Surface Modification. All reagents employed for surface modification were of reagent grade, and they were used as received from Aldrich unless otherwise stated. The patterned quartz chips were cleaned in an RCA cleaning solution [$H_2O/NH_4OH/30\%$ H_2O_2 (5:1:1, vol/vol)] for 15 min at 70°C, immersed in a water bath for 10 min, and dried in a stream of argon. The quartz surface was coated with a hydrophobic octadecyltriethoxysilane (Gelest, Morrisville, PA) in an anhydrous toluene solution containing 1% (vol/vol) silane and 2% (vol/vol) hexanoic acid for 24 h at room temperature. Silanized chips were washed twice with toluene and once with ethanol for 5 min each and dried in a stream of argon. The silanization step was performed to make the quartz surface hydrophobic and thereby avoid crosscontamination between gold electrodes in close proximity to each other during spotting.

The gold electrodes were coated with a long-chain thiol that forms a densely packed monolayer and displaces any physisorbed silanes (23, 24). The silane-coated chips were immersed immediately in a 1 mM solution of mercaptoundecanol in ethanol for at least 16 h. The gold substrates were removed from the thiol solution, washed with ethanol, and dried under an argon stream. The hydroxyl-terminated monolayer was transformed into a thiol-reactive moiety by exposure to a 2.3 mM solution of *N*-(*p*-maleimidophenyl) isocyanates (Pierce) in anhydrous toluene at 40°C for 2 h under an argon atmosphere (25, 26). Maleimide-modified gold electrodes were washed with anhydrous toluene and dried in a stream of argon. The various surface modification steps were followed by x-ray photoelectron spectroscopy (data not shown), and the presence of the expected elements and peak shifts confirmed the proper transformation of both surface components.

Immobilization of DNA. The thiolated oligonucleotides were diluted to a final concentration of 10 μM in 0.1 M phosphate buffer, pH 7.4, with 10 μM DTT, and they were then incubated for at least 1 h at room temperature. Immobilization of the reduced thiolated oligonucleotides onto the electrodes was performed manually by deposition of 0.2 μl of reduced oligonucleotides followed by overnight incubation at room temperature in a humidified chamber.

Design, Synthesis, and Purification of Oligonucleotides. Single-stranded DNA molecules (76 bases) with different sequences were chemically synthesized with a thiol modification on the 5′ terminus and HPLC-purified by MWG Biotech (High Point, NC). The DNA sequences were designed to self-prime with a 19-bp self-complementary sequence at the 5′ end of the DNA. Approximately 40 bases of the DNA sequence were single-stranded and extendable by DNA polymerase. The oligonucleotide used in the experiment (Fig. 1*A*) was 5′-thiol/TTTTTTTTTTTTTTTTTTTTTGCTGGAATTCGTCAGTGACGCCGTCGTTTTACAACGGAACGGCAGCAAAATGTTGC.

Prototype Sensor System. In a typical charge-based sensor system, a prefabricated electrode matrix is used for DNA immobilization. The electrodes were fabricated as described above. Fig. 1*C* shows the top view of a CPD electrode chip that was used in these experiments.

The electrode surface was submersed in a standard DNA polymerization buffer (5 mM Tris·HCl, pH 8.3/25 mM KCl/1.25 mM $MgCl_2$) with DNA polymerase (10 units, KF). Polymerization was initiated by adding a 2-μl aliquot containing 20 mM dNTP substrate (to give a 1 mM final concentration of dNTP in 40 μl of buffer).

Electrical Measurement Method. For measurements of electrical activity of the CPD electrode we used an Axopatch 200B voltage-clamp amplifier (Axon Instruments). The Axopatch amplifier was used in the whole-cell voltage-clamp mode with the holding potential at 0 mV. The high-impedance coating of the CPD measurement electrode prevents the occurrence of faradaic current that could otherwise cause interference or the deterioration of the sensor and analytes. A reference Ag/AgCl electrode of the voltage-clamp amplifier was immersed directly in the bathing solution during measurements.

Radiolabeling. Radioactive labeling and phosphorimaging techniques were used to quantify the oligonucleotide attachment and for subsequent hybridization reactions (27). [α-^{32}P]dCTP (Amersham Pharmacia) was used for 3′ labeling of the attached self-primed probes by single-base extension. Specific activities of the radiolabeled oligonucleotides were determined by liquid scintillation counting with an LS 7500 liquid scintillation system (Beckman). Standard curves were made from a serial dilution of known amounts of the ^{32}P-labeled nucleotides used in the experiments. The data presented here represent the averages of at least three replicate points.

We thank Prof. Robert Lehman for invaluable discussions. A.Z. was supported in part by a Howard Hughes Medical Institute International Research Scholar Award. This work was supported by National Institutes of Health Grants 1R21 A1059499-01 and HG 000205.

1. Kuchta, R. D., Benkovic, P. & Benkovic, S. J. (1988) *Biochemistry* **27,** 6716–6725.
2. Johnson, K. A. (1995) *Methods Enzymol.* **249,** 38–61.
3. Patel, S. S., Wong, I. & Johnson, K. A. (1991) *Biochemistry* **30,** 511–525.
4. Sawaya, M. R., Prasad, R., Wilson, S. H., Kraut, J. & Pelletier, H. (1997) *Biochemistry* **36,** 11205–11215.
5. Bockris, J. O. M., Reddy, A. K. N. & Gamboa-Aldeco, M. (1998) *Modern Electrochemistry* (Plenum, New York), pp. 820–827.
6. Sadiku, M. N. O. (2001) *Elements of Electromagnetics* (Oxford Univ. Press, New York), pp. 240–242.
7. Lide, D. R. (1999) *CRC Handbook of Chemistry and Physics* (CRC, London), Sect. 5, pp. 93–95.
8. Gutman, M. & Nachliel, E. (1997) *Annu. Rev. Phys. Chem.* **48,** 329–356.
9. Georgievskii, Y., Medvedev, E. S. & Stuchebrukhov, A. A. (2002) *Biophys. J.* **82,** 2833–2846.
10. Wong, I., Patel, S. S. & Johnson, K. A. (1991) *Biochemistry* **30,** 526–537.
11. Davenport, R. J., Wuite, G. J., Landick, R. & Bustamante, C. (2000) *Science* **287,** 2497–2500.
12. Purohit, V., Grindley, N. D. & Joyce, C. M. (2003) *Biochemistry* **42,** 10200–10211.
13. Zhong, X., Patel, S. S., Werneburg, B. G. & Tsai, M. D. (1997) *Biochemistry* **36,** 11891–11900.
14. Dahlberg, M. E. & Benkovic, S. J. (1991) *Biochemistry* **30,** 4835–4843.
15. Arndt, J. W., Gong, W., Zhong, X., Showalter, A. K., Liu, J., Dunlap, C. A., Lin, Z., Paxson, C., Tsai, M. D. & Chan, M. K. (2001) *Biochemistry* **40,** 5368–5375.
16. Melamede, R. J. (1985) U.S. Patent 4,863,849.
17. Ronaghi, M., Uhlen, M. & Nyren, P. (1998) *Science* **281,** 363, 365.
18. Franca, L. T., Carrilho, E. & Kist, T. B. (2002) *Q. Rev. Biophys.* **35,** 169–200.
19. Drummond, T. G., Hill, M. G. & Barton, J. K. (2003) *Nat. Biotechnol.* **21,** 1192–1199.

20. Fritz, J., Cooper, E. B., Gaudet, S., Sorger, P. K. & Manalis, S. R. (2002) *Proc. Natl. Acad. Sci. USA* **99,** 14142–14146.
21. Fan, C., Plaxco, K. W. & Heeger, A. J. (2005) *Trends Biotechnol.* **23,** 186–192.
22. Dubin, A. E., Nasser, N., Rohrbacher, J., Hermans, A. N., Marrannes, R., Grantham, C., Van Rossem, K., Cik, M., Chaplan, S. R., Gallacher, D., *et al.* (2005) *J. Biomol. Screen.* **10,** 168–181.
23. Lan, S., Veiseh, M. & Zhang, M. (2005) *Biosens. Bioelectron.* **20,** 1697–1708.
24. Yuk, J. S., Jung, S. H., Jung, J. W., Hong, D. G., Han, J. A., Kim, Y. M. & Ha, K. S. (2004) *Proteomics* **4,** 3468–3476.
25. Robinson, D. B., Persson, H. H., Zeng, H., Li, G., Pourmand, N., Sun, S. & Wang, S. X. (2005) *Langmuir* **21,** 3096–3103.
26. Persson, H. H. J., Caseri, W. R. & Suter, U. W. (2001) *Langmuir* **17,** 3643–3650.
27. Miyahara, J. (1989) *Chem. Today* **223,** 29–36.
28. Ramanathan, S., Chary, K. V. & Rao, B. J. (2001) *Nucleic Acids Res.* **29,** 2097–2105.
29. Kunkel, T. A. & Bebenek, K. (2000) *Annu. Rev. Biochem.* **69,** 497–529.
30. Allbritton, N. L., Meyer, T. & Stryer, L. (1992) *Science* **258,** 1812–1815.